# Electronic, optical properties, surface energies and work functions of $Ag_8SnS_6$: First-principles method*

Lu Chun-Lin(卢春林)[a], Zhang Lin(张 林)[a)b)†], Zhang Yun-Wang(张云望)[a], Liu Shen-Ye(刘慎业)[a], and Mei Yang(梅 杨)[c]

[a] *Science and Technology on Plasma Physics Laboratory, Research Center of Laser Fusion, China Academy of Engineering Physics, Mianyang* 621900, *China*
[b] *Jointment Laboratory for Extreme Conditions Matter Properties, Southwest University of Science and Technology Research Center of Laser Fusion, China Academy of Engineering Physics, Mianyang* 621010, *China*
[c] *School of Physics and Electronic Engineering, Mianyang Normal University, Mianyang* 621000, *China*

(Received 14 April 2014; revised manuscript received 4 September 2014; published online 25 November 2014)

Ternary metal chalcogenide semiconductor $Ag_8SnS_6$, which is an efficient photocatalyst under visible light radiation, is studied by plane-wave pseudopotential density functional theory. After geometry optimization, the electronic and optical properties are studied. A scissor operator value of 0.81 eV is introduced to overcome the underestimation of the calculation band gaps. The contribution of different bands is analyzed by virtue of total and partial density of states. Furthermore, in order to understand the optical properties of $Ag_8SnS_6$, the dielectric function, absorption coefficient, and refractive index are also performed in the energy range from 0 to 11 eV. The absorption spectrum indicates that $Ag_8SnS_6$ has a good absorbency in visible light area. Surface energies and work functions of $(\bar{4}11)$, $(4\bar{1}3)$, $(21\bar{1})$, and (112) orientations have been calculated. These results reveal the reason for an outstanding photocatalytic activity of $Ag_8SnS_6$.

**Keywords:** density functional theory, $Ag_8SnS_6$, optical properties, surface energy

**PACS:** 75.15.Mb, 71.20.–b, 78.20.Ci, 65.40.gh **DOI:** 10.1088/1674-1056/24/1/017501

## 1. Introduction

Organic pollutants are an important composition in dye wastewater. Nowadays, dyes have been widely used in textile industry, leather tanning industry, paper production, etc. Over one million tons of dyes are produced each year. How to degrade the dyes has become a worldwide problem.[1] In particular, the photocatalysis is a kind of potential technique for removing the hazardous organic contaminants from sewage. Accordingly, preparation of effective photocatalyts has been a hot topic.[2,3] Most photocatalysts (such as $TiO_2$,[4] ZnO,[5] and ZnS[6]) have catalysis only under ultraviolet (UV) radiation. However, almost 43% of the solar radiation energy is in visible light area (400–750 nm), and only 4% comes from UV radiation.[7] Syntheses of photocatalyts, which have high catalytic activity under visible light radiation, are in pressing requirement.

$Ag_8SnS_6$ is a narrow band gap semiconductor, and its band energy gap is 1.39 eV.[8] Because its valence band contains S 3p orbital, it has good photocatalytic activity under visible light radiation. As reported in Ref. [9], $Ag_8SnS_6$ shows superior catalytic capability compared to commercial $TiO_2$ under visible light radiation. The $E_g$ of $Ag_8SnS_6$ was first reported by Osipishi in 1972,[8] and the structure was released by Wang in 1978.[10] The optical UV–vis absorption spectrum was measured by An *et al.*[9] $Ag_8SnS_6$ has a strong absorption spike in the visible region. However, to the best of our knowledge, there are no theoretical works to explain their electronic and optical properties. Hence, in order to obtain a further understanding of $Ag_8SnS_6$, theoretical investigation on the structural, electronic, and optical properties is necessary. In the present work, the electronic and optical properties, surface energies and work functions of $Ag_8SnS_6$ are investigated by performing the density functional theory (DFT) with generalized gradient approximation (GGA) and local density approximation (LDA).

## 2. Details of computational method

All the calculations were performed within the density functional theory, using the plane-wave pseudopotential scheme. The generalized gradient approximation (GGA) with the Perdew–Burke–Ernzerhof (PBE) functional was used to treat the exchange-correlation effects.[11–14] The electron function was expanded in the plane-wave basis set with a cutoff energy of 350 eV. Broyden–Fletcher–Goldfarb–Shanno (BFGS) scheme was used for *k*-point sampling in geometry optimization.[15] The Monkhorst–Pack *k*-points grid sampling was set at 2×4×2 points for the first Brillouin zone. The convergence tolerance parameters are set as follows: energy, less than $5.0 \times 10^{-6}$ eV/atom; maximum atoms force, less than 0.05 eV/Å; maximum stress, less than 0.02 GPa; maximum displacement, less than $5.0 \times 10^{-4}$ Å. The Ag $4d^{10}5s^1$, Sn $5s^25p^2$, and S $3s^23p^4$ electrons were explicitly treated as valence electrons. In calculation of surface energies and work functions, the $(\bar{4}11)$, $(4\bar{1}3)$, $(21\bar{1})$, and (112) planes were

*Project supported by the Science and Technology Development Foundation of China (Grant Nos. 2012A0302015 and 2012B0302050).
†Corresponding author. E-mail: zhlmy@sina.com
© 2015 Chinese Physical Society and IOP Publishing Ltd 

cleaved and set as surface. The local-density approximation with the Caperley–Alder–Perdew–Zunger parameterization (LDA-CA-PZ) and GGA-PBE exchange correlation functionals were used for these calculations.[13,16] The parameters were set the same as bulk calculation. In surface energies calculation, the slab fractional thickness was set as 3, and a vacuum layer width of 12.0 Å was employed. The slab fractional thickness of 3.0 and vacuum thickness of 30.0 Å were used for work function calculation.[17–21] The $k$ points of models $(\bar{4}11)$, $(4\bar{1}3)$, $(21\bar{1})$, and (112) were set as $1 \times 2 \times 2$, $1 \times 1 \times 2$, $1 \times 2 \times 1$, and $1 \times 1 \times 2$, respectively. All the calculations were performed using the CASTEP code.

## 3. Results and discussion

### 3.1. Structure of $Ag_8SnS_6$

According to the literature, $Ag_8SnS_6$ belongs to *Pna*21 space group of the orthorhombic crystal system.[10] It contains four formula units in a single unit cell. There are two different types of S atoms in the $Ag_8SnS_6$ crystal structure. The first type connects Sn and Ag atoms together, and the other only form a bond with Ag atoms. The crystal structure of $Ag_8SnS_6$ is presented in Fig. 1. The equilibrium structural parameters were determined by using the Birch–Murnaghan equation.[22,23] The $Ag_8SnS_6$ structure was optimized with the given parameters in Section 2. Experimental data are compared with geometry optimization results (see Table 1). Experimental[10] and calculated values of the lattice parameters match with each other very well. The optimized structure was used to calculate electronic and optical properties in the next section.

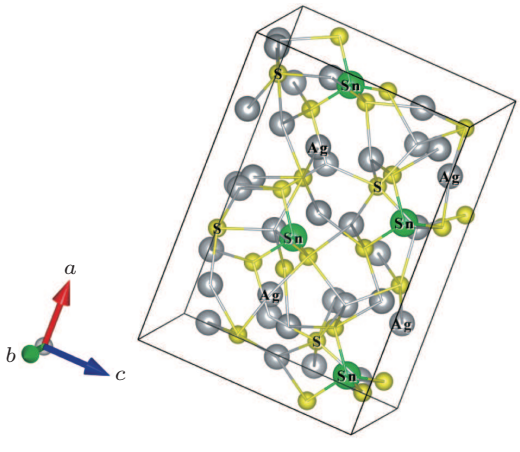



**Fig. 1.** (color online) Structure of $Ag_8SnS_6$.

**Table 1.** Experimental and calculated crystal structure parameters of $Ag_8SnS_6$.

| | $a$/Å | $b$/Å | $c$/Å | $V$/Å$^3$ |
|---|---|---|---|---|
| Experimental data | 15.2980 | 7.5480 | 10.6990 | 1235.41 |
| Calculation results | 15.4883 | 7.65393 | 10.8697 | 1288.56 |

### 3.2. Electronic properties

The band structure of $Ag_8SnS_6$ is shown in Fig. 2. $Ag_8SnS_6$ is a direct band gap semiconductor, and the conduction band minimum and the valence band maximum are at the G point. The band gap is about 0.58 eV, which is obviously less than the experimental value of 1.39 eV. The underestimated energy band gap values often come forth in the calculated simulation. This is related to the DFT limitations, and it does not take into account the discontinuity in the exchange–correlation potential.[24] For the sake of resolving this incongruity, the scissors operator is introduced.[15,25] It can eliminate the difference between the experimental and calculated data, and shift the unoccupied conduction band with respect to the valence band. The scissors operator at 0.81 eV was performed in the present work. Table 2 shows band gap energies along with the valence to conduction band transition of $Ag_8SnS_6$. As we know, when the irradiation photon energy is greater than the semiconductor band gap, the electron will be excited to create an electron–hole pair. Photons exhibit a wavelike character with the wavelength ($\lambda$), which is related to the photon energy $E_\lambda$ by

$$E_\lambda = hc/\lambda, \tag{1}$$

where $h$ is Plank's constant, and $c$ is the speed of light.[26] Therefore, in order to use visible light, the $E_g$ of semiconductors should be below 3.0 eV (above 400 nm).[27] The narrower the energy band gap, the excited electrons and holes separate and migrate more easily. Because $Ag_8SnS_6$ has the narrow band gap of 1.39 eV, the electrons in the valence band of $Ag_8SnS_6$ are easily excited to the conduction band under visible light radiation. Consequently, $Ag_8SnS_6$ has excellent photocatalytic capability in the visible light area.

**Table 2.** Symmetry of the valence to conduction band transition of $Ag_8SnS_6$. VB: valence band; CB: conduction band.

| | | CB | | | | | | | |
|---|---|---|---|---|---|---|---|---|---|
| | | $G$ | $Z$ | $T$ | $Y$ | $S$ | $X$ | $U$ | $R$ |
| VB | $G$ | 1.39 | 1.51 | 1.54 | 1.42 | 1.49 | 1.45 | 1.52 | 1.48 |
| | $Z$ | 2.35 | 2.48 | 2.50 | 2.39 | 2.45 | 2.41 | 2.48 | 2.45 |
| | $T$ | 2.59 | 2.72 | 2.75 | 2.63 | 2.70 | 2.66 | 2.73 | 2.69 |
| | $Y$ | 2.01 | 2.14 | 2.17 | 2.05 | 2.12 | 2.08 | 2.14 | 2.11 |
| | $S$ | 2.82 | 2.95 | 2.98 | 2.86 | 2.93 | 2.89 | 2.95 | 2.92 |
| | $X$ | 2.73 | 2.86 | 2.89 | 2.77 | 2.84 | 2.80 | 2.87 | 2.83 |
| | $U$ | 2.72 | 2.85 | 2.88 | 2.76 | 2.83 | 2.78 | 2.85 | 2.82 |
| | $R$ | 2.84 | 2.97 | 3.00 | 2.88 | 2.95 | 2.91 | 2.97 | 2.94 |

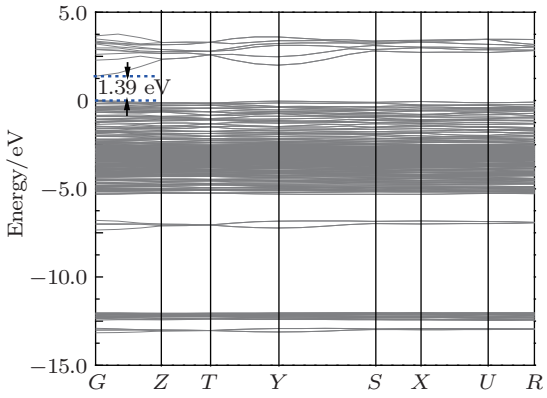



**Fig. 2.** Calculated band structure of $Ag_8SnS_6$.

The partial and total density of states (PDOS and TDOS) can be used to analyze the composition of the energy bands. The DOS of $Ag_8SnS_6$ is presented in Fig. 3. The conduction band between 1.40 eV and 3.80 eV is contributed from Ag 5s and 5p states, Sn 5s and S 3p states, and these states are hybridized. The valence band is split into four sub-bands. In the uppermost valence band, Ag 4d, S 3p, and a small quantity of Sn 5p states are observed between 0 and −5.40 eV. The second sub-band is contributed from Sn 5s and S 3p states, which is from −6.80 eV to −7.30 eV. The third one locates at 12.00–12.40 eV, which consists of Ag 4d, Ag 5s, Ag 5p, Sn 5p, S 3s, and S 3p states. The lowest one is from −12.70 eV to 13.00 eV. It is the main contribution of S 3s state, Sn 5s states, and Ag 4d, 5s, 5p states.

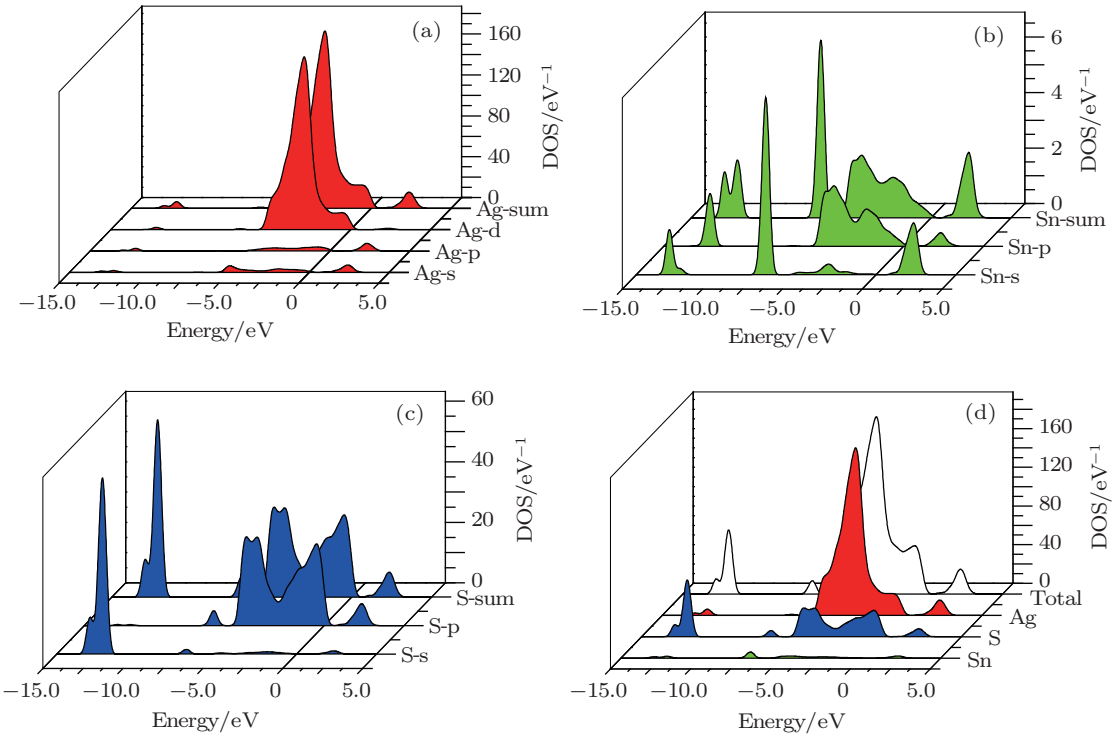



**Fig. 3.** (color online) Calculated partial and total density of states of $Ag_8SnS_6$.

The charge density has been studied, and it was used to analyze the electronic structure of the system. The charge density distribution of $Ag_8SnS_6$ in (040) plane is displayed in Fig. 4. The covalent bond of materials can be associated with the sharing of the electrons between the atoms. As seen in Fig. 4, there is a distinct continuity in the constant charge contours among Ag, Sn, S atoms. The charge accumulations are presented between S and Ag, Sn atoms. These indicate that covalent bonds are formed between Ag and S atoms, Sn and S atoms.

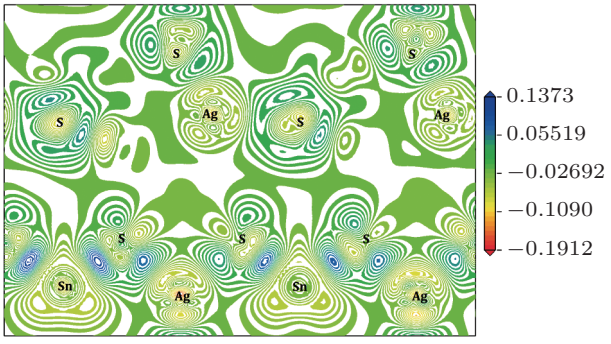



**Fig. 4.** (color online) Charge density of $Ag_8SnS_6$ in (040) plane.

### 3.3. Optical properties

The dielectric function is used to describe the optical properties of solid material. The dielectric constant $\varepsilon$ is given by

$$\varepsilon(\omega) = \varepsilon_1(\omega) + \mathrm{i}\varepsilon_2(\omega), \tag{2}$$

where $\varepsilon_1$ and $\varepsilon_2$ are the real and imaginary part of the dielectric function, respectively. The $\varepsilon_2(\omega)$ can be used to describe the detail of the transitions between occupied and unoccupied electronic states, and the adsorptive behavior of materials. It is given by [15,28]

$$\varepsilon_2(\omega) = \frac{(2e^2\pi)}{\omega\varepsilon_0}\sum_{k,v,c}|\langle\Psi_k^c|\boldsymbol{u}\cdot\boldsymbol{r}|\Psi_k^v\rangle|^2 \times\delta(E_k^c - E_k^v - E), \tag{3}$$

where $\boldsymbol{u}$ is the vector defining the polarization of the incident electric field, $\boldsymbol{r}$ is the electron's radius vector, $e$ is the electric charge, $\Psi_k^c$ and $\Psi_k^v$ are the wave functions of the conduction band and valence band, $E$ is the incident photon's energy, and $\varepsilon_0$ is the dielectric permittivity of vacuum. The real part of $\varepsilon_1(\omega)$ can be obtained by following the Kramers–Kronig relationship.[29,30]

$$\varepsilon_1(\omega) = 1 + \frac{2}{\pi}P\int_0^{+\infty}\frac{\varepsilon_2(\omega')\omega'\,\mathrm{d}\omega'}{\omega'^2 - \omega^2}, \tag{4}$$

where $P$ is the principal value of the integral, defined as

$$P = \lim_{a\to 0}\int_{-\infty}^{\omega-a}\frac{\varepsilon(\omega')}{\omega'-\omega}\,\mathrm{d}\omega' + \lim_{a\to 0}\int_{\omega+a}^{+\infty}\frac{\varepsilon(\omega')}{\omega'-\omega}\,\mathrm{d}\omega'. \tag{5}$$

The complex dielectric functions of different polarizations and polycrystalline are displayed in Fig. 5. Polycrystalline values are averaged over all polarization directions. The static dielectric constant $\varepsilon_1(0)$ is 4.15 at zero frequency limit. Because there is negative scale from 3.97 eV to 9.15 eV, it indicates that the $Ag_8SnS_6$ has a metallic behavior in these energy zones. As seen from Fig. 5(b), there are five peaks which are marked by the symbols A (2.89 at 1.96), B (3.08 at 2.64), C (8.05 at 3.51), D (2.34 at 6.40), and E (1.38 at 7.02). The peak A is due to the electronic transition from S 3s (at −6.90 eV) to Ag 5s (at −4.96 eV), S 3p (at −4.85 eV to −2.89 eV), S 3p (at −6.91 eV) to Ag 5s (at −4.96 eV), Sn 5s (at −4.96 eV) to Ag 5s (at −6.90 eV) and Sn 5p (at −4.81 eV) to Ag 4d (at −2.89 eV). Peak B is contributed from Sn 5p (at −4.36 eV) to Ag 5s (at −1.89 eV). Peak C is mainly due to the transition from S 3p (at −6.91 eV) to Ag 5p (at −3.46 eV) and Sn 5s (at −6.90 eV) to Ag 5p (at −3.46 eV). Peak D originates from S 3p (at −6.91 eV) to Ag 4d (at −0.54 eV), S 3s (at −6.90 eV) to S 3p (at −0.47 eV), S 3s (at −6.90 eV) to Ag 4d (at −0.54 eV) and Sn 5s (at −6.90 eV) to Ag 4d (at −0.54 eV). Peak E may be due to transition from Sn 5p (at −12.10 eV) to Ag 5s (at −4.96 eV) and Ag 4d (at −12.16 eV) to Ag 5p (at −4.96 eV).

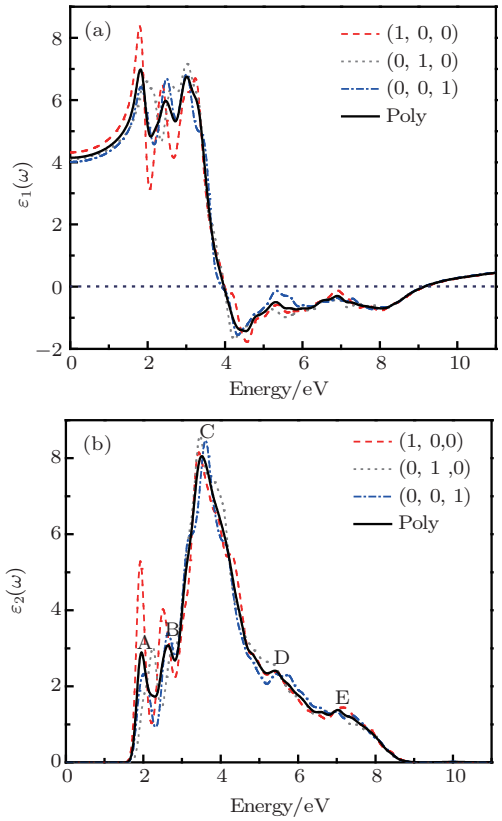



**Fig. 5.** (color online) Calculated dielectric function $\varepsilon$ for $Ag_8SnS_6$ in different polarization and polycrystalline. (a) Real part $\varepsilon_1(\omega)$; (b) imaginary part $\varepsilon_2(\omega)$.

The refractive index $n$ and $Ag_8SnS_6$ with different polarizations are presented in Fig. 6. The estimation of the refractive index is carried out by extracting square root of $\varepsilon_1(\omega)$ in the limit of infinite wavelengths. The static refractive index $n(0)$ of three polarizations are as follows: $n(1,0,0) = 2.08$, $n(0,1,0) = 2.03$, and $n(0,0,1) = 2.00$, the gap between them is very small. The trend of these curves are the same, all of them have 3 peaks from 400 nm to 700 nm. The maximum $n$ of (1, 0, 0), (0, 1, 0), and (0, 0, 1) polarizations are 2.80 at 683 nm, 2.80 at 404 nm, and 2.74 at 407 nm, respectively. The $n(0)$ of polycrystalline is 2.04, and the maximum $n$ is 2.72 at 405 nm.

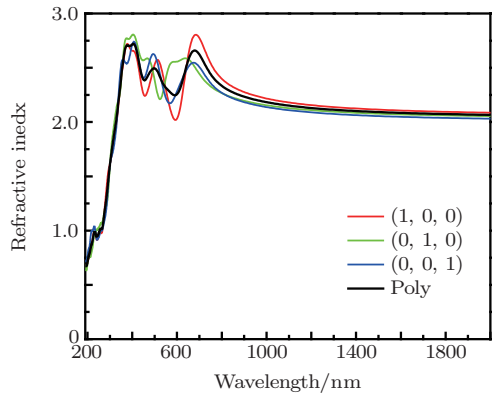



**Fig. 6.** (color online) Refractive index of $Ag_8SnS_6$ in different polarization and polycrystalline.

$Ag_8SnS_6$ is a significant photocatalyst, so the absorption coefficient is one of the most important parameters for measuring its catalytic activity. The calculated absorption spectrum of polycrystalline $Ag_8SnS_6$ is depicted in Fig. 7. It shows a wide absorbency from 190 nm to 750 nm, especially in the ultraviolet range (190–400 nm), the absorption coefficient is almost above $8 \times 10^4$ cm$^{-1}$. It also shows a good adsorption in the visible light area (400–750 nm), and the absorption coefficient locates at about $1 \times 10^4$–$1.5 \times 10^4$ cm$^{-1}$. Comparison with the absorption spectrum of experiments in Ref. [9], the curves of these two spectrums have the same tendency in visible light area. However, the experimental data indicated that it has a weak absorption in the infrared region from 750 nm to 1350 nm. This difference might be related to the experiment conditions, the spectra were obtained by testing the nanocrystalline $Ag_8SnS_6$, while the calculation results were carried out by using the bulk $Ag_8SnS_6$. However, this evidence can explain that $Ag_8SnS_6$ has a marked catalysis activity under visible light radiation.

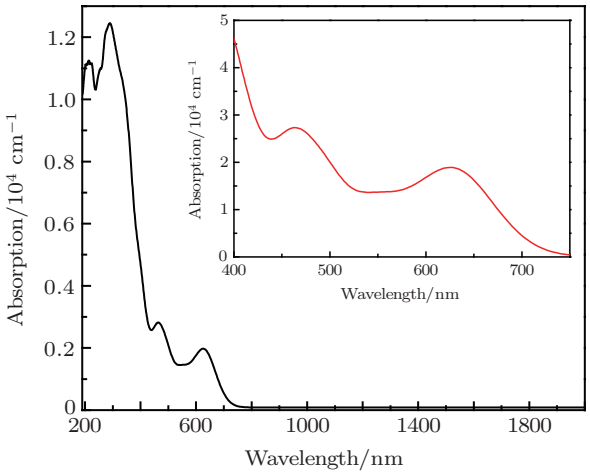



**Fig. 7.** (color online) Absorption spectrum of $Ag_8SnS_6$.

As seen in Fig. 8, the optical conductivity $\sigma(\omega)$, loss function $L(\omega)$, and reflectivity $R(\omega)$ are displayed. Optical conductivity of a semiconductor is associated with the change in conductivity caused by illumination, either an increase or a decrease. Generally, the optical conductivity is the physical basis of optoelectronic applications of semiconductors. It contains the absorptive $\sigma_1(\omega)$ (real part) and reactive $\sigma_2(\omega)$ (imaginary part) current response to a time-varying external electrical field of frequency. The optical conductivity $\sigma(\omega)$ is displayed in Fig. 8(a). The real part of optical conductivity is zero when the energy is less than 1.46 eV and greater than 11.39 eV, and the peak is 3.52 fs$^{-1}$ at 3.60 eV. In the imaginary part, $\sigma_2(\omega)$ value is zero at 7.56 eV.

The loss function is a significance parameter describing the energy lost by an electron passing through a homogeneous dielectric material. The peak of loss function spectrum relates to the plasma resonance, and the corresponding frequency is called plasma frequency $\omega_p$. Figure 8(b) shows that the resonant energy locates at 9.25 eV. The reflection coefficient can be obtained for the simple case of normal incidence onto a plane surface by matching both the electric and magnetic fields at the surface. Reflectivity $R(\omega)$ is shown in Fig. 8(c). The $R(0)$ is 11.5%, and the maximum reflectivity value is 66.10% at 9.08 eV. The $Ag_8SnS_6$ has a good reflective ability in the ultraviolet and visible light area (190–750 nm). The small value of reflectivity as well as absorptivity in the infrared region indicates that $Ag_8SnS_6$ is transparent in this range.

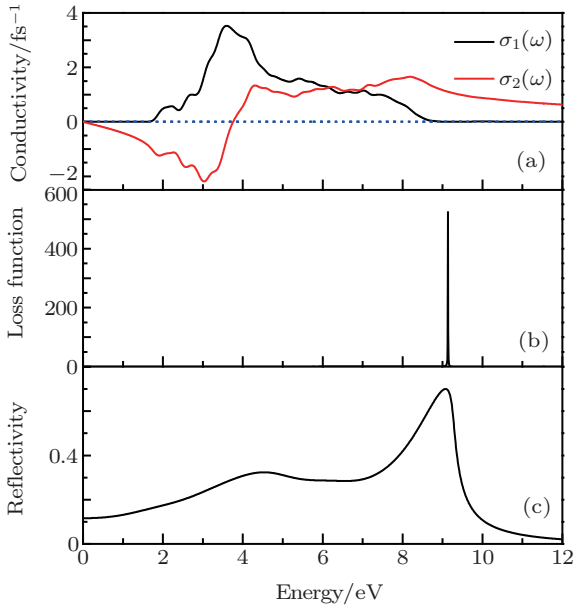



**Fig. 8.** (color online) Optical spectrum of $Ag_8SnS_6$. (a) Optical conductivity. (b) Energy loss function. (c) Reflectivity.

### 3.4. Surface energies and work functions

The photocatalytic reactions occur at the surface of $Ag_8SnS_6$ nanocrystal. So the surface energy is an important factor to influence the photocatalytic activity. The surface energy is the energy required to create a new surface, and it is difficult to measure in the experiment. Generally, the surface energies are determined at the melting temperature. In the calculation, the surface energy $\gamma$ can be calculated by taking the energy difference between the total energy of a slab and a bulk reference amount

$$\gamma = \frac{E_{\text{slab}} - nE_{\text{bulk}}}{2A}, \tag{6}$$

where $E_{\text{slab}}$ and $E_{\text{bulk}}$ are the total energies of slab and bulk per unit cell, respectively, $n$ is the number of unit cells in slab, and $A$ is the surface area.[31]

As seen from the literature, the nanocrystalline $Ag_8SnS_6$ have a submicropyramids structure, and its four outer faces correspond to $(\bar{4}11)$, $(4\bar{1}3)$, $(21\bar{1})$, and (112) planes. These four surfaces were constructed by cleaving on the planes (Fig. 9). Firstly, the GGA and LDA exchange correlation

functional were performed for determining $E_{\text{bulk}}$. The energies of slab were carried out using the same parameters as $E_{\text{bulk}}$ calculation. The surface energies were calculated by using Eq. (6). The results are shown in Table 3. Experimental values of $Ag_8SnS_6$ surface energies have not been reported up to now. So we compared our presented GGA and LDA values with the calculated results from literature. It can be seen from Table 3, the $(21\bar{1})$ surface has the maximum surface energy of 2.76 J/m$^2$ with GGA calculated and 3.02 J/m$^2$ with LDA. The $(\bar{4}11)$ with PBE and LDA calculations had the minimum energy of 1.11 and 1.42 J/m$^2$, respectively. The GGA calculation results seemed to underestimate surface energies. The LDA values were about 0.25 J/m$^2$ larger than PBE. Presented work surface energies were quite different from literature results. This might relate to the different module and different parameters used in simulation. The Dmol3 module was performed in the surface energies calculation in Ref. [9]. As reported in Ref. [17], a conclusion that LDA was the better choice of exchange correlation functional than GGA for surface energies calculation was obtained, because the LDA results were closer to experimental values.

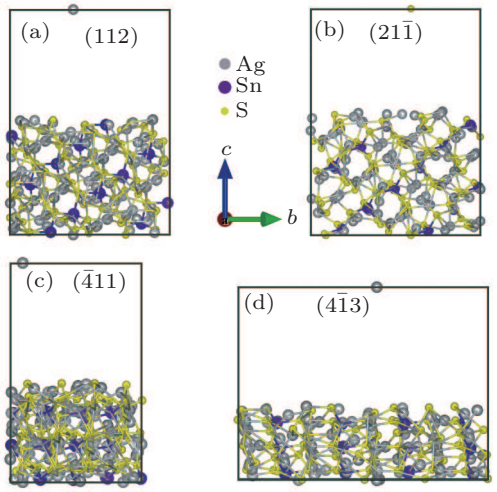



**Fig. 9.** (color online) Surface models of (a) (112), (b) $(21\bar{1})$, (c) $(\bar{4}11)$, and (d) $(4\bar{1}3)$ orientation of $Ag_8SnS_6$.

**Table 3.** Surface energies (J/m$^2$) and work functions (eV) of $Ag_8SnS_6$ four different surfaces.

| | | $(\bar{4}11)$ | $(4\bar{1}3)$ | $(21\bar{1})$ | (112) |
|---|---|---|---|---|---|
| Surface energy/J·m$^{-2}$ | GGA | 1.59 | 1.11 | 2.76 | 1.46 |
| | LDA | 1.80 | 1.41 | 3.02 | 1.84 |
| | Ref. [9] | 2.16 | 0.74 | 0.83 | 1.31 |
| Work function/eV | GGA | 4.706 | 4.559 | 4.415 | 4.524 |
| | LDA | 4.874 | 4.663 | 4.604 | 4.733 |

The work function is the minimum energy required removing an electron from a solid to a point immediately outside the solid surface, or the energy needed to move an electron from the Fermi energy level into a vacuum. The expression is shown as follows:

$$\Phi = -e\phi - E_{\text{F}}, \tag{7}$$

where $\Phi$ is work function, $-e$ is the charge of an electron, $\phi$ is the electrostatic potential in the vacuum near the surface, and $E_{\text{F}}$ is the Fermi level inside the material.[32]

Usually, this energy depends on the orientation of the crystal; different orientation surfaces have different work function values. As we know, in the photocatalytic reaction, the first step is that electrons move outside from the $Ag_8SnS_6$ surface under the light radiation. The mechanism can be expressed as follows: $Ag_8SnS_6 + h\nu \rightarrow e^-$. Therefore, the work function is a significant parameter for estimating the catalytic activity of $Ag_8SnS_6$. Experimental and calculated work function values of $Ag_8SnS_6$ have not been reported yet. As seen from Table 3, GGA and LDA values were determined. The results of all four orientations were approximately at 4.5 eV. These values have little difference between each other. The $(21\bar{1})$ surface has the minimum work function of 4.415 eV, and the $(4\bar{1}3)$ surface has the maximum value of 4.706 eV with GGA evaluated. In LDA calculation, these two surfaces' work functions are 4.604 and 4.874 eV, respectively. As for the surface energies, the work function values with LDA are bigger than GGA, and the LDA results are closer to the actual values. The LDA exchange correlation functional is a good choice for surface energy and work function calculating. These calculation values can be used as a reference for determination of experimental values.

## 4. Conclusion

Firstly, the structure of $Ag_8SnS_6$ is optimized, and the electronic and optical properties are calculated by performing the density functional theory (DFT) with the generalized gradient approximation (GGA). In order to eliminate the error of underestimation of calculation band gaps, a scissor operator of 0.81 eV is introduced. Dielectric function, absorption spectrum and refractive index are used to study the optical properties. Interestingly, the absorption spectra indicate that $Ag_8SnS_6$ has an excellent absorptivity in visible light area. The static refractive index $n(0)$ of polycrystalline is 2.04. Next, surface energies and work functions of $(\bar{4}11)$, $(4\bar{1}3)$, $(21\bar{1})$, and (112) surfaces are calculated by GGA and LDA exchange correlation functionals, respectively. As seen from the results, the values, which are evaluated with LDA, are larger than the results calculated with GGA. These four surfaces have a high surface energy, which offers a good activity for adsorbing and degrading organic contaminations. The work functions of four faces are approximately 4.5 eV, and they have little difference. The work functions could be used to investigate the photocatalytic activity of $Ag_8SnS_6$.

## References

[1] Forgacs E, Cserhati T and Oros G 2004 *Environ. Int.* **30** 953
[2] Kudo A and Miseki Y 2009 *Chem. Soc. Rev.* **38** 253

[3] Hoffmann M R, Martin S T, Choi W and Bahnemann D W 1995 *Chem. Rev.* **95** 69
[4] Fujishima A, Rao T N and Tryk D A 2000 *J. Photoch. Photobio. C* **1** 1
[5] Afzaal M, Malik M A and O'Brien P 2007 *New J. Chem.* **31** 2029
[6] Hu J S, Ren L L, Guo Y G, Liang H P, Cao A M, Wan L J and Bai C L 2005 *Angew. Chem.* **117** 1295
[7] Silva L A, Ryu S Y, Choi J, Choi W and Hoffmann M R 2008 *J. Phys. Chem. C* **112** 12069
[8] Osipishi I, Butsko N I, Gasii B I and Zhezhnic I D 1972 *Sov. Phys. Semicond.* 974
[9] Hu W Q, Shi Y F and Wu L M 2012 *Cryst. Growth Des.* **12** 3458
[10] Wang N 1978 *Neues Jahrbuch Für Mineralogie, Monatshefte* 269
[11] Perdew J P, Burke K and Ernzerhof M 1996 *Phys. Rev. Lett.* **77** 3865
[12] Perdew J P and Zunger A 1981 *Phys. Rev. B* **23** 5048
[13] Yousaf M, Saeed M A, Isa A R M, Aliabad H A R and Sahar M R 2013 *Chin. Phys. Lett.* **30** 077402
[14] Yangthaisong A 2013 *Chin. Phys. Lett.* **30** 077101
[15] Brik M G 2013 *J. Phys. Condens. Matter* **25** 345802
[16] Shojaei A R, Nourbakhsh Z, Vaez A and Dehghani M 2013 *Chin. Phys. B* **22** 127102
[17] Singh-Miller N E and Marzari N 2009 *Phys. Rev. B* **80** 235407
[18] Zhang J M, Ma F and Xu K W 2004 *Chin. Phys.* **13** 1082
[19] He M C and Zhao J 2013 *Chin. Phys. B* **22** 016802
[20] Li R, Zhong Y, Huang C, Tao X and Ouyang Y 2013 *Physica B* **422** 51
[21] Rák Z, Ewing R C and Becker U 2013 *Surf. Sci.* **608** 180
[22] Liang H N, Ma C L, Du F, Cui Q L and Zou G T 2013 *Chin. Phys. B* **22** 016103
[23] Liu L, Wei J J, An X Y, Wang X M, Liu H N and Wu W D 2011 *Chin. Phys. B* **20** 106201
[24] Sun B and Zhang P 2008 *Chin. Phys. B* **17** 1364
[25] Sesion Jr P D, Henriques J M, Barboza C A, Albuquerque E L, Freire V N and Caetano E W S 2010 *J. Phys. Condens. Matter.* **22** 435801
[26] Luque A and Hegedus S 2011 *Handbook of Photovoltaic Science and Engineering* (2nd edn.) (Hoboken: John Wiley & Sons, Inc.) p. 82
[27] Chen X, Shen S, Guo L and Mao S S 2010 *Chem. Rev.* **110** 6503
[28] Li Z L, An X Y, Cheng X L, Wang X M, Zhang H, Peng L P and Wu W D 2014 *Chin. Phys. B* **23** 037104
[29] Zhang L Y, Yan J L, Zhang Y J and Li T 2012 *Chin. Phys. B* **21** 067102
[30] Liu Q J, Liu Z T, Che X S, Feng L P and Tian H 2011 *Solid State Sci.* **13** 2177
[31] Yu J, Lin X, Wang J, Chen J and Huang W 2009 *Appl. Surf. Sci.* **255** 9032
[32] Kittel C 1986 *Introduction to Solid State Physics* (8th edn.) (Hoboken: John Wiley & Sons, Inc.) p. 494